International Journal of Environmental Sciences
ISSN: 2229-7359
Vol. 11 No. 21s, 2025
https://theaspd.com/index.php

Development And Optimization of Baricitinib -Nanoparticle Loaded Transdermal Patches for Treatment in Rheumatoid Arthritis

Mr. Bharat V. Jadhav[1], Dr. Sanjay Bhawar.[2]
[1]Research Scholar, Bhagwant University, Ajmer, India
[2]Professor and Principal, Pravara Rural College of Pharmacy, Loni, Maharashtra, India

Corresponding author
Mr. Bharat V. Jadhav[1]
Address: Research Scholar, Bhagwant University, Ajmer, India
bjpharma302@gmail.com

Abstract

Objectives: *The study aimed to develop and optimize Baricitinib-loaded nanoparticles (BCT-NPs) for incorporation into a transdermal patch to improve drug bioavailability and ensure controlled drug release.* ***Methods:*** *Nanoparticles were prepared using the nanoprecipitation method with Eudragit RL100 and DMSO. A 3^2 factorial design was employed to optimize key formulation parameters such as polymer concentration and solvent volume. BCT-NPs were characterized for particle size, entrapment efficiency (EE), and zeta potential. The optimized batch was incorporated into a hydrogel-based transdermal patch and evaluated for physicomechanical and release properties. In vitro release kinetics and accelerated stability studies were also conducted.* ***Results:*** *The optimized batch (NF5) demonstrated a particle size of 116.6 ± 10.3 nm, entrapment efficiency of 79.67 ± 2.45%, and zeta potential of –39.32 mV. Among transdermal patches, TNF2 exhibited superior performance with optimal tensile strength (1.432 ± 0.07 kg/cm²), folding endurance (193 ± 1.21), and cumulative drug release of 83.29% at 12 h. Zero-order kinetics (R^2 = 0.9816) best described the release profile. Accelerated stability testing confirmed the formulation's physical and chemical stability over three months.* ***Conclusion:*** *The factorial-optimized BCT-NPs loaded transdermal patch demonstrated effective drug encapsulation, sustained release, and robust mechanical properties. This formulation holds potential for enhancing the clinical management of Baricitinib therapy via non-invasive, patient-compliant delivery. Further in vivo studies are warranted to confirm its therapeutic applicability and bioavailability improvements.*

Keywords: *Baricitinib, Nanoparticles, Transdermal Patch, 3^2 Factorial Design, Sustained Release, Stability Study.*

INTRODUCTION

Rheumatoid arthritis (RA) is a chronic autoimmune disorder affecting nearly 1% of the global population, with higher prevalence among females and the elderly [1]. According to the World Health Organization, over 20 million people worldwide are affected by RA, leading to substantial disability and diminished quality of life [2]. The economic burden is immense, with direct healthcare costs and productivity losses exceeding $46 billion annually in the U.S. alone. Current treatment regimens, including NSAIDs, corticosteroids, and biologics, provide symptomatic relief but are associated with significant drawbacks such as systemic toxicity, poor bioavailability, and frequent dosing [3]. Oral administration, in particular, often results in gastrointestinal disturbances and hepatic metabolism-related degradation, necessitating higher doses and increasing adverse effects [4]. Despite recent advancements in biologics and small molecule inhibitors, long-term efficacy and patient compliance remain challenging. Moreover, invasive administration routes like subcutaneous injections further limit acceptance. These limitations underscore the urgent need for a non-invasive, efficient, and sustained drug delivery system for long-term RA management [5].

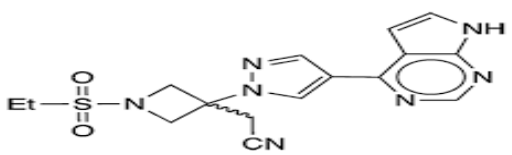

Figure 1: Baricitinib

Baricitinib, a selective Janus kinase (JAK1/JAK2) inhibitor, has emerged as a promising therapeutic agent for the management of moderate to severe RA [6]. Its molecular structure ($C_{16}H_{17}N_7O_2S$) supports high specificity in modulating the JAK-STAT signaling pathway, thereby attenuating cytokine-mediated inflammatory responses implicated in RA pathogenesis. Baricitinib inhibits the phosphorylation and activation of downstream transcription factors, reducing synovial inflammation and joint damage [7]. Studies have shown that baricitinib effectively improves Disease Activity Score (DAS28) and ACR20 response rates compared to traditional DMARDs, with a favorable oral bioavailability of ~80%. However, oral delivery poses limitations due to first-pass metabolism and fluctuation in plasma levels [8]. Several clinical investigations have supported baricitinib's efficacy, but patient adherence and adverse systemic effects remain concerns [9]. Its small molecular weight (~371.4 g/mol) and lipophilic nature (logP ≈ 2.4) make it a suitable candidate for transdermal delivery. These attributes, combined with its potent anti-inflammatory action, present a compelling case for reformulating baricitinib into a controlled-release topical system [10].

Transdermal drug delivery systems (TDDS) offer an attractive alternative to oral and parenteral routes, enabling sustained release, enhanced bioavailability, and improved patient compliance [11]. In this study, nanoparticle-loaded transdermal patches were selected to deliver baricitinib efficiently across the skin barrier. Nanoparticles, particularly polymeric types, can encapsulate drugs, protect them from degradation, and enhance permeation through stratum corneum due to their nanoscale size and surface characteristics [12]. Incorporating baricitinib into nanoparticles facilitates controlled release and minimizes systemic side effects. Additionally, the TDDS platform circumvents hepatic first-pass metabolism and provides consistent plasma drug levels, reducing dosing frequency [13]. Recent innovations in nanotechnology-based TDDS have demonstrated success with lipophilic drugs, showing improved pharmacokinetics and therapeutic indices. Moreover, patch formulations ensure non-invasive, painless administration, with potential for self-application and better adherence [14]. The synergistic combination of nanotechnology and transdermal delivery aligns with current pharmaceutical trends aimed at optimizing chronic disease management. Thus, this approach holds significant potential for revolutionizing RA therapy through enhanced delivery of JAK inhibitors [15].

The present study aims to develop and optimize baricitinib-loaded nanoparticle-based transdermal patches for effective RA treatment. Specific objectives include formulation of nanoparticles, characterization, incorporation into patches, and evaluation of physicochemical, ex vivo, and in vitro release profiles. The study seeks to overcome bioavailability challenges while offering a patient-friendly, sustained delivery system to enhance therapeutic outcomes and reduce systemic side effects.

MATERIALS AND METHODS

MATERIALS

Baricitinib (analytical grade, MW 371.42 g/mol) was obtained from Sciquaint Innovations. (Pune, India). Eudragit® RL100 (pharmaceutical grade) was procured from Evonik Industries (Mumbai, India). Polyvinyl alcohol (PVA, analytical grade, 30–70 cps) and dimethyl sulfoxide (DMSO, HPLC grade, ≥99.9%) were supplied by Loba Chemie Pvt. Ltd. (Mumbai, India). Methanol (HPLC grade, ≥99.8%) was purchased from Merck Ltd. (Mumbai, India). HPMC K15M (pharmaceutical grade) and polyvinylpyrrolidone (PVP K30, MW ~40,000 Da) were obtained from Sigma-Aldrich (St. Louis, USA). PEG 400 (analytical grade) and dialysis membrane (MWCO 12–14 kDa) were obtained from Himedia (Mumbai, India). All other reagents used were of analytical grade.

METHODS

Calibration curve determination

A calibration curve for Baricitinib was developed using a UV-Visible spectrophotometer (Shimadzu UV-1900, Kyoto, Japan) for accurate quantitative analysis. A stock solution of 100 µg/mL was prepared by dissolving 10 mg of Baricitinib in methanol and diluting to 100 mL with the same solvent. From this, working solutions in the range of 5 to 30 µg/mL were prepared by serial dilution with methanol. Absorbance of each solution was measured at 252 nm against methanol as blank at 25 ± 2 °C. All measurements were performed in triplicate (n = 3). A calibration curve was plotted with concentration on the X-axis and absorbance on the Y-axis. The linear regression equation and correlation coefficient ($R^2 > 0.999$) confirmed excellent linearity. The method adhered to ICH Q2(R1) guidelines and was found suitable for Baricitinib quantification in analytical procedures [16].

Solubility study

The solubility of Baricitinib was determined in various solvents methanol, ethanol, distilled water, phosphate buffer pH 6.8, and dimethyl sulfoxide (DMSO) using the solvent saturation method. Excess amount of Baricitinib was added to 10 mL of each solvent in separate glass vials, which were then sealed and stirred using a magnetic stirrer (Remi Equipments, India) at 25 ± 2 °C for 24 hours to attain equilibrium. After equilibration, the mixtures were filtered through 0.45 µm membrane filters to remove undissolved drug. The filtrates were appropriately diluted with their respective solvents, and the drug concentration was measured using a UV-Visible spectrophotometer (Shimadzu UV-1900, Kyoto, Japan) at 252 nm. All experiments were performed in triplicate (n = 3). The solubility values were calculated in mg/mL, allowing comparative evaluation of Baricitinib solubility across different solvents for use in formulation selection [17,18].

Differential scanning calorimetry

Differential Scanning Calorimetry (DSC) was performed to evaluate the thermal behavior and compatibility of Baricitinib with excipients. Samples of pure drug, individual excipients (HPMC K15M, Eudragit RL100, PEG 400), and their physical mixture were analyzed using a DSC instrument (DSC 4000, PerkinElmer, USA). Accurately weighed samples (2–5 mg) were sealed in aluminum pans and heated from 30 °C to 300 °C at a rate of 10 °C/min under nitrogen flow (40 mL/min). An empty aluminum pan served as the reference. Thermograms were examined for melting point, peak shifts, or disappearance to assess drug–excipient interactions. All tests were performed in triplicate (n = 3) for consistency [19,20].

Fourier Transform Infrared (FTIR)

Fourier Transform Infrared (FTIR) spectroscopy was carried out to evaluate possible interactions between Baricitinib and formulation excipients. FTIR spectra of pure drug, individual excipients (HPMC K15M, Eudragit RL100, PEG 400), and their physical mixture were recorded using an FTIR spectrometer (Alpha II, Bruker, Germany) equipped with an ATR (attenuated total reflectance) accessory. About 1–2 mg of each sample was placed directly on the crystal surface, and spectra were scanned over a range of 4000–400 cm^{-1} at a resolution of 4 cm^{-1} with 32 scans per sample. Characteristic peaks of functional groups were compared across the samples to detect any significant shifts, disappearance, or new peak formation indicating potential interactions. All analyses were performed in triplicate (n = 3) to ensure reproducibility [21,22].

Experimental design

A full 3^2 factorial design was employed to optimize the formulation parameters of Baricitinib-loaded nanoparticles using two independent variables X1: concentration of Eudragit RL100 (200, 225, 250 mg) and X2: volume of DMSO (10, 15, 20 mL) each at three levels, resulting in nine experimental runs. The selected responses were R1: particle size (nm) and R2: entrapment efficiency (%), which are critical for assessing formulation performance. This design enabled the evaluation of both individual and interactive effects of the variables. Statistical optimization and model fitting were performed using Design-Expert® software, employing a second-order polynomial regression equation of the form:

$$\mathbf{Y = \beta_0 + \beta_1 X_1 + \beta_2 X_2 + \beta_{12} X_1 X_2 + \beta_{11} X_1^2 + \beta_{22} X_2^2},$$

Where Y = response (R1 or R2), β_0 = intercept, β_1 and β_2 = linear coefficients, β_{12} = interaction coefficient, β_{11} and β_{22} = quadratic coefficients, and X_1 and X_2 are coded levels of Eudragit RL100 and DMSO volume, respectively [23-25].

Table 1: Layout of Two Factor Three Level Design

Independent Variables						
Factors	**Coded Values**			**Actual Values (mg)**		
X_1 - Eudragit RL100	-1	0	+1	200	225	250
X_2 - Volume of DMSO	-1	0	+1	10	15	20
Dependent Variables (Response)						
R1- Particle Size (nm)						
R2- Entrapment Efficiency (%)						

Preparation of Baricitinib Nanoparticles (BCT-NPs)

Baricitinib-loaded nanoparticles were prepared using a modified nanoprecipitation method based on the procedure reported by Parmanand Verma et al. Accurately weighed quantities of Eudragit RL100 (200–250 mg) were dissolved in 10–20 mL of DMSO to form the organic phase. Separately, an aqueous

phase containing 1% w/v polyvinyl alcohol (PVA) was prepared. The aqueous phase was added dropwise to the organic phase under continuous magnetic stirring at 10,000 rpm at room temperature, leading to spontaneous formation of nanoparticles indicated by slight turbidity. The mixture was subjected to solvent evaporation under reduced pressure at 58 °C to remove residual DMSO. To eliminate large aggregates, the nanoparticle suspension was filtered through a 1.2 µm cellulose nitrate membrane filter [26,27].

Table 2: Composition of Baricitinib Nanoparticle Formulations (BCT-NPs)

Batch Code	Eudragit RL100 (mg)	DMSO Volume (mL)	PVA (1% w/v)
F1	200	10	20 mL
F2	200	15	20 mL
F3	200	20	20 mL
F4	225	10	20 mL
F5	225	15	20 mL
F6	225	20	20 mL
F7	250	10	20 mL
F8	250	15	20 mL
F9	250	20	20 mL

Evaluations of Nanoparticles

Entrapment Efficiency (EE)

The entrapment efficiency (% EE) of Baricitinib nanoparticles (BCT-NPs) was determined indirectly by quantifying the amount of unentrapped drug. A known volume of nanoparticle suspension was placed in 2 mL centrifuge tubes and centrifuged using a high-speed refrigerated centrifuge (KUBOTA 7000, Japan) at 35,000 rpm and 4 °C for 60 minutes. The clear supernatant was collected, suitably diluted with phosphate buffer pH 6.8, and analyzed using a UV-Visible spectrophotometer (Shimadzu UV-1900, Kyoto, Japan) at 252 nm to determine the concentration of free drug. The percentage entrapment efficiency was calculated using the formula [28]:

$$\% \text{ EE} = \frac{\text{Amount. of drug added} - \text{unentrapped drug}}{\text{Amount of drug added}} \times 100 \qquad (1)$$

Particle size analysis and zeta potential measurement

Dynamic Light Scattering (DLS) was employed to determine the particle size distribution and zeta potential (ZP) of Baricitinib nanoparticles using a computerized inspection system (Zetasizer Nano ZS, Malvern Instruments, Malvern, UK). The nanoparticle suspension was appropriately diluted with distilled water and injected into the measurement cell. Measurements were performed in multimodal analysis mode with a run time of 200 seconds per replicate at a medium stable count rate. The analysis was conducted in triplicate (n = 3), and the average particle size (in nm) and zeta potential (in mV) were recorded to assess colloidal stability and uniformity [29].

In-vitro drug release studies

The in vitro drug release profile of Baricitinib nanoparticles (BCT-NPs) was evaluated over a 12-hour period using the dialysis bag diffusion technique. A cellulose acetate dialysis membrane (MWCO 12–14 kDa, Sigma-Aldrich, USA) was pre-soaked and used to enclose 1 mL of BCT-NPs dispersion. The bag was securely sealed at both ends and immersed in 100 mL of phosphate buffer saline (PBS, pH 6.8) contained in an amber glass beaker, maintained at 37 ± 0.5 °C and stirred continuously at 100 rpm using a magnetic stirrer. To minimize evaporation, the beaker was covered with a lid. At predetermined intervals, aliquots were withdrawn from the dissolution medium and immediately replaced with an equal volume of fresh PBS to maintain sink conditions. The drug concentration in each sample was determined using a UV-Visible spectrophotometer (Shimadzu UV-1900, Kyoto, Japan) at 252 nm. All experiments were conducted in triplicate (n = 3) to ensure reproducibility of the release data [30].

Preparation of the Baricitinib Nanoparticle (BCT-NPs) loaded transdermal patch

Baricitinib-loaded transdermal patches were prepared using the solvent casting technique. Accurately weighed quantities of HPMC K15M and polyvinylpyrrolidone (PVP) were dispersed in boiled distilled water and stirred using a magnetic stirrer (Remi, India) until a homogeneous gel-like solution was obtained. The required amount of dried Baricitinib nanoparticles (BCT-NPs) was added to this polymeric solution and further stirred for 20 minutes to ensure uniform dispersion. Polyethylene glycol (PEG 400) was added as a plasticizer in varying concentrations (0.5%, 1%, and 2%), with the total

plasticizer content ranging from 1% to 5%. The final formulation was poured onto a glass petri plate of 7.9 cm internal diameter (area = 48.99 cm^2), and the solvent was allowed to evaporate at 37 ± 0.5 °C with 40 ± 5% relative humidity. An inverted funnel was placed over the setup to prevent rapid solvent loss, allowing uniform film formation [31].

Table 3: Composition of Baricitinib Nanoparticle (BCT-NPs) loaded transdermal patch

Sr. No.	Ingredients	TNF1	TNF2	TNF3	TNF4
1	Baricitinib Nanoparticle (equivalent to) mg	2	2	2	2
2	HPMC K15M (mg)	50	100	150	200
3	PVP (mg)	50	100	200	300
4	PRG 400 (%)	0.5	1	1.5	2
5	Methanol : Water (2:1) (ml)	10	10	10	10

Evaluation of Transdermal Patches [8,9]

Thickness Measurement

The thickness of the transdermal patches was measured using a digital vernier caliper at five different points on each patch. The patches were placed between points of vernier caliper, and the thickness was recorded to the nearest 0.001 mm. The mean thickness and standard deviation were calculated for all the patches [32].

Weight Uniformity

The weight uniformity of the Baricitinib-loaded transdermal patches was assessed by individually weighing ten randomly selected patches using an analytical balance (Mettler Toledo, India). Each patch was weighed carefully, and the mean weight along with standard deviation was calculated to ensure batch uniformity. The mean weight was determined using the formula [33]:

$$\text{Mean weight} = \Sigma \frac{(\text{weight of individual patches})}{10} \quad (2)$$

Folding Endurance

The folding endurance of the Baricitinib-loaded transdermal patches was determined by repeatedly folding each patch at the same point until it either broke or withstood up to 300 continuous folds without breaking. The total number of folds the patch endured before breaking was recorded as its folding endurance. This test was performed in triplicate (n = 3) for each formulation to evaluate the mechanical flexibility and durability of the patches [34].

Tensile Strength

The tensile strength of the Baricitinib-loaded transdermal patches was measured using a texture analyzer (TA.XT Plus, Stable Micro Systems, UK). Each patch was clamped securely between the upper and lower grips, and a uniaxial force was applied at a constant rate until the patch ruptured. The maximum force required to break the patch was recorded. From the resulting stress-strain curve, tensile strength, elongation at break, and modulus of elasticity were calculated. Tensile strength was calculated using the formula [35]:

$$\text{Tensile strength } (N/mm^2) = \frac{\text{Maximum load (N)}}{\text{Initial cross} - \text{sectional area } (mm^2)} \quad (3)$$

Drug Content Uniformity

The drug content of the Baricitinib-loaded transdermal patches was determined by dissolving a predetermined area of each patch in a suitable volume of methanol. The resulting solution was filtered through a 0.45 µm membrane filter to remove any undissolved components. The absorbance of the clear filtrate was measured at 252 nm using a UV-Visible spectrophotometer (Shimadzu UV-1900, Japan) against a methanol blank. The concentration of Baricitinib was determined from the calibration curve, and the drug content was expressed in µg/cm^2. The analysis was carried out in triplicate (n = 3), and the mean drug content and standard deviation were calculated using the formula [37]:

$$\text{Mean drug content } (\mu g/cm^2) = \frac{\Sigma\ (\text{drug content of individual samples})}{3} \quad (4)$$

In vitro Permeation Studies

The in vitro drug release study of Baricitinib-loaded transdermal patches was performed using a Franz diffusion cell apparatus (PermeGear, USA) to evaluate the release profile across a semipermeable membrane. A patch with a known surface area was placed in the donor compartment, while the receptor compartment was filled with 20 mL of phosphate buffer pH 6.8, maintained at 37 ± 0.5 °C and stirred

continuously using a magnetic stirrer. At specific time intervals, 1 mL aliquots were withdrawn from the receptor medium and immediately replaced with an equal volume of fresh buffer to maintain sink conditions. The withdrawn samples were analyzed at 252 nm using a UV-Visible spectrophotometer (Shimadzu UV-1900, Japan). All measurements were performed in triplicate (n = 3), and the cumulative percentage drug release was calculated to determine the release kinetics [38].

Release kinetics

The release kinetics of Baricitinib from the transdermal patches were evaluated by fitting the in vitro release data to zero-order, first-order, Higuchi, and Korsmeyer–Peppas models. Data analysis was performed using Microsoft Excel, and the correlation coefficient (R^2) was calculated for each model to determine the best fit. Zero-order, first-order, and Higuchi models were used to assess constant, concentration-dependent, and diffusion-based release, respectively, while the Korsmeyer–Peppas model helped identify the release mechanism through the release exponent (n). The model with the highest R^2 value was considered most suitable, and all evaluations were done in triplicate (n = 3) [39].

RESULTS AND DISCUSSION

Calibration curve determination

The calibration curve of Baricitinib in methanol exhibited excellent linearity over the concentration range of 5–30 µg/mL. The regression equation obtained was y = 0.0242x + 0.0035 with a high correlation coefficient (R^2 = 0.9998), indicating a strong linear relationship between concentration and absorbance. This confirms the suitability of the developed UV-spectrophotometric method for accurate drug quantification in further formulation analysis.

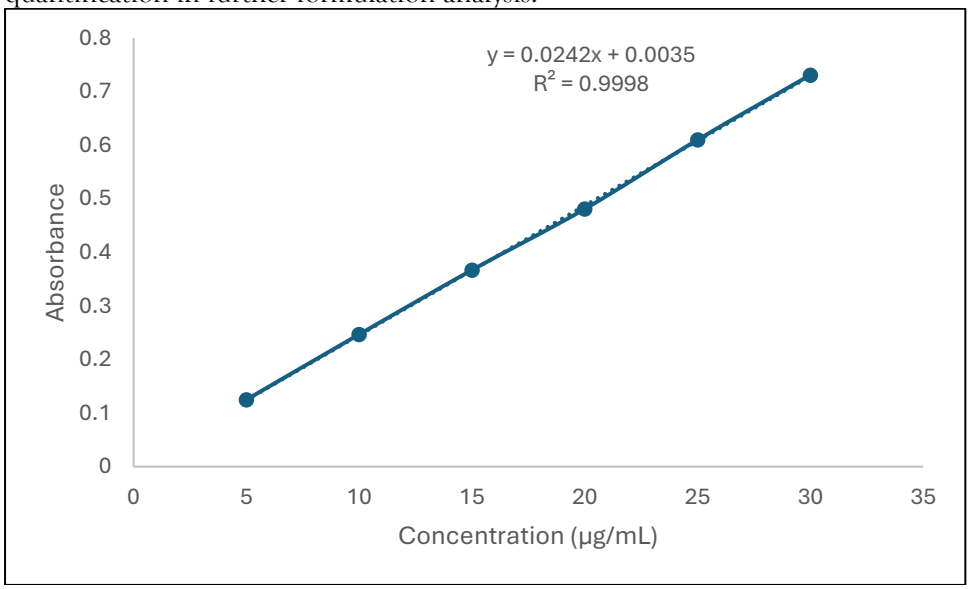

Figure 2: Calibration Curve of Baricitinib in Methanol

Solubility study

The solubility of Baricitinib was evaluated in different solvents using the saturation solubility method. DMSO exhibited the highest solubility (74.0 ± 1.0 mg/mL), classifying it as freely soluble. Methanol showed moderate solubility (21.4 ± 0.6 mg/mL), indicating sparingly soluble behavior. Ethanol, phosphate buffer pH 6.8, and distilled water demonstrated very slight solubility (<0.5 mg/mL). These results confirm Baricitinib's poor aqueous solubility (Table 4), justifying the need for nanoparticle-based formulation.

Table 4: Results of solubility study

Solvent	Mean ± SD (mg/mL)	Inferred Solubility Class
DMSO	74.0 ± 1.0	Freely Soluble
Methanol	21.4 ± 0.6	Sparingly Soluble
Ethanol	0.40 ± 0.05	Very Slightly Soluble
Phosphate Buffer (pH 6.8)	0.46 ± 0.04	Very Slightly Soluble
Distilled Water	0.36 ± 0.03	Very Slightly Soluble

All values are expressed as mean±SD

International Journal of Environmental Sciences
ISSN: 2229-7359
Vol. 11 No. 21s, 2025
https://theaspd.com/index.php

Differential scanning colorimetry

The DSC thermogram of pure Baricitinib displayed a sharp endothermic peak at 214.94°C, confirming its crystalline nature. In contrast, the physical mixture showed broadened peaks at 149.79°C and 216.62°C, indicating partial interaction between Baricitinib and excipients without complete amorphization. The presence of drug peak in the mixture suggests no significant incompatibility (Figure 3).

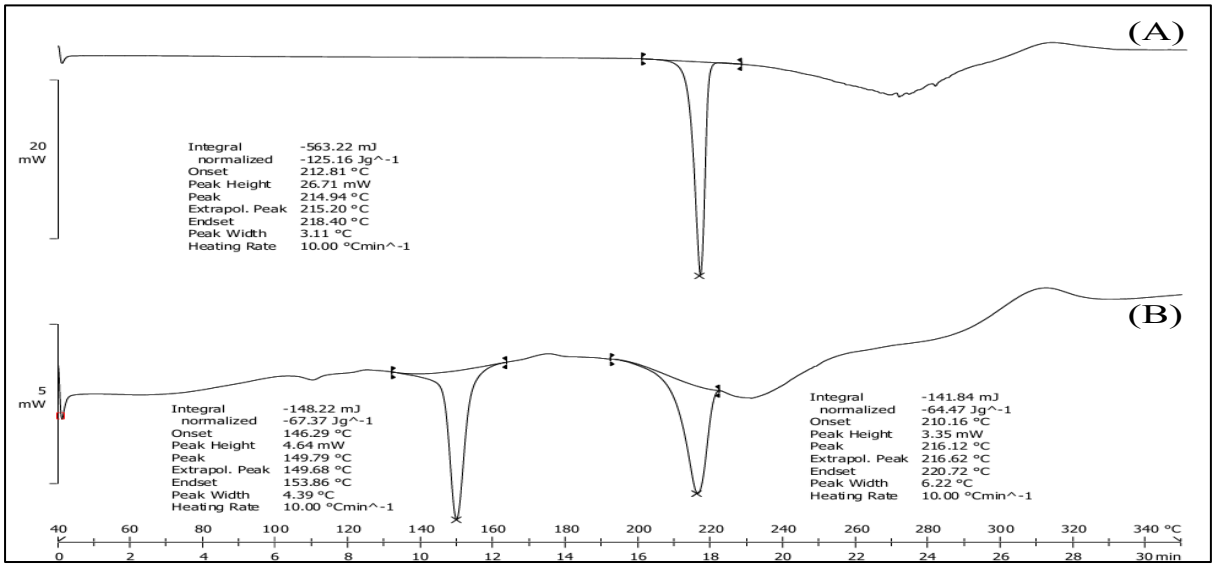

Figure 3: DSC spectra of (A) pure Baricitinib (214.94°C) (B) Physical mixture (149.79°C and 216.62°C)

FTIR analysis

FTIR analysis of pure Baricitinib (Figure 4A) revealed distinct characteristic peaks at 3539.7 cm^{-1} (O–H stretching), 2978.42 cm^{-1} (C–H stretching), and 1655.59 cm^{-1} (C=O stretching), indicative of intact functional groups. The physical mixture spectrum (Figure 4B) also showed corresponding absorption bands, such as peaks at 3596.56 cm^{-1} and 1747.19 cm^{-1}, without significant shifts, disappearance, or formation of new peaks. This similarity in spectral features between pure drug and its mixture confirms the absence of any strong chemical interaction and supports the compatibility between Baricitinib and excipients used in the nanoparticle formulation.

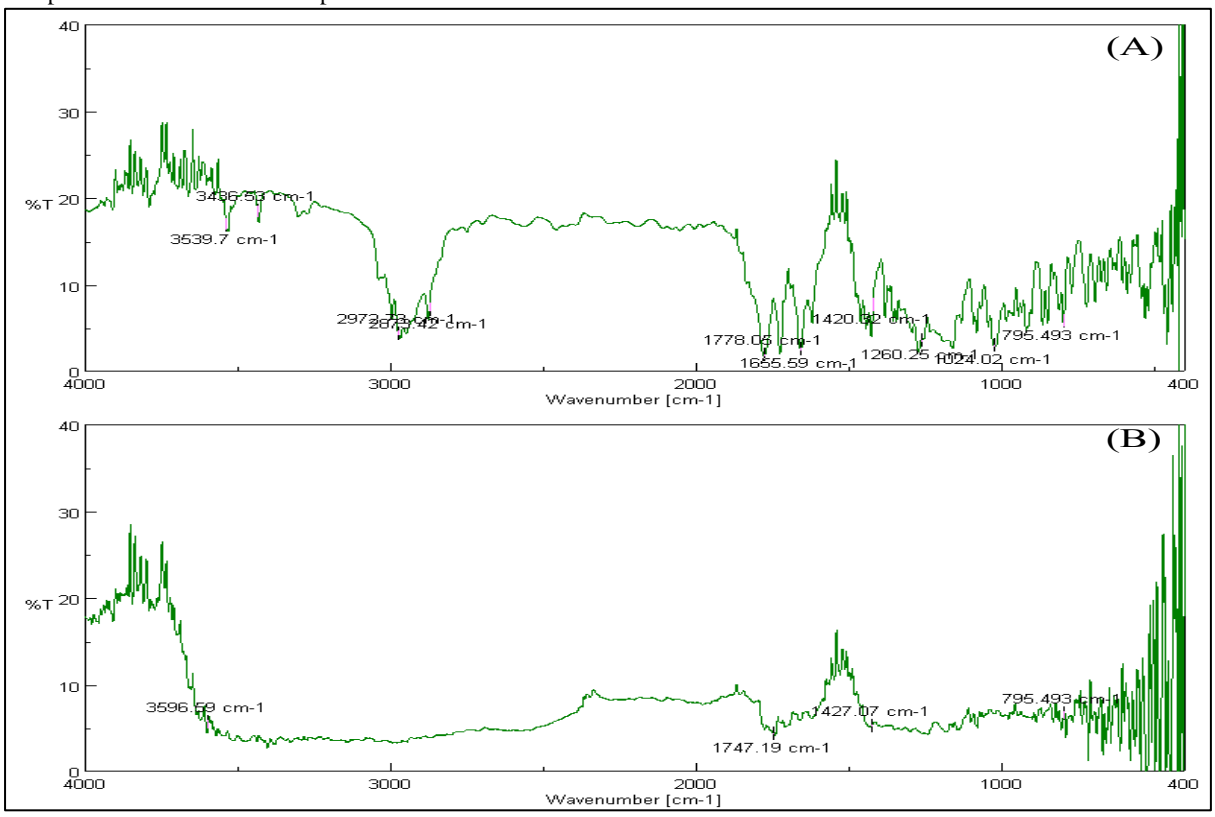

Figure 4: FTIR Spectra of (A) Pure baricitinib drug (B) Physical mixture

Evaluations of Baricitinib Nanoparticle (BCT-NPs)

As shown in Table 5, the particle size of the prepared Baricitinib-loaded nanoparticles (BCT-NPs) ranged from 116.6 ± 10.3 nm (NF5) to 148.4 ± 21.6 nm (NF3), indicating a nanoscale size suitable for enhanced permeation. The highest entrapment efficiency was observed in NF3 (89.92 ± 3.45%), while the lowest was noted in NF9 (60.57 ± 0.78%), suggesting the influence of formulation parameters on drug loading. Zeta potential values ranged from -24.54 mV to -44.85 mV, with NF9 demonstrating the highest negative surface charge, indicating better colloidal stability. These results confirm successful nanoparticle formation with acceptable size, drug retention, and electrostatic stability.

Table 5: Results of Entrapment Efficiency and Particle Size for prepared Baricitinib Nanoparticle (BCT-NPs)

Batch	Particle Size (nm)	Entrapment Efficiency (%)	Zeta potential (mV)
NF1	139.8±18.3	78.76±1.78	-24.54
NF2	134.3±12.6	81.31±2.23	-36.43
NF3	148.4±21.6	89.92±3.45	-37.19
NF4	131.4±13.5	79.32±1.23	-33.24
NF5	116.6±10.3	79.67±2.45	-39.32
NF6	132.2±25.3	80.12±2.67	-27.77
NF7	144.9±31.6	82.28±3.32	-37.58
NF8	123.3±17.3	68.43±2.56	-32.71
NF9	137.3±10.5	60.57±0.78	-44.85

Values are expressed in mean±SD, (n=3)

Optimization of Baricitinib Nanoparticle (BCT-NPs)

Effect of Formulation Variables on Particle Size (R1)

The particle size of Baricitinib-loaded nanoparticles was evaluated as a key response variable and modeled using a quadratic polynomial equation. The ANOVA results (Table 7) revealed that the model was statistically significant with an F-value of 20.92 and a corresponding p-value of 0.0154, indicating the adequacy of the model to represent the data. The model's reliability was further supported by a high R^2 value of 0.9925, an adjusted R^2 of 0.9800, and a predicted R^2 of 0.9097 (Table 6), confirming good agreement between experimental and predicted values. The low standard deviation (2.18) and coefficient of variation (0.9377%) further validate model precision. Among the individual terms, the quadratic components A^2 (F = 54.92, p = 0.0051) and B^2 (F = 34.25, p = 0.0099) were statistically significant, whereas the linear terms A (p = 0.8047) and B (p = 0.0840), along with the interaction term AB (p = 0.0588), were not statistically significant at $p < 0.05$ but exhibited observable effects on the response.

The regression equation derived for particle size was:

Particle size (R1) = 117.22 + 0.3000A – 2.83B – 4.05AB + 14.27A^2 + 11.27B^2

The coefficients indicate that particle size was positively influenced by quadratic terms of both Eudragit RL100 concentration and DMSO volume, while the linear and interaction terms showed comparatively smaller effects. The contour plot and 3D response surface plot (Figures 5A and 5B) demonstrated a nonlinear relationship, with the smallest particle size observed at moderate Eudragit RL100 levels and lower DMSO volumes. The predicted vs. actual plot showed a close alignment along the line of identity, confirming model predictability. The perturbation plot further confirmed that DMSO volume exerted a slightly greater effect than Eudragit RL100 concentration on particle size within the studied range.

Effect of Formulation Variables on Entrapment Efficiency (R2)

Entrapment efficiency of Baricitinib nanoparticles was statistically analyzed using a quadratic model. The ANOVA findings (Table 7) indicated that the model was significant with an F-value of 20.73 and a p-value of 0.0156, suggesting the model's robustness in capturing the variability in the response. The model's fit was further supported by an R^2 value of 0.9719, adjusted R^2 of 0.9250, and an adequate precision value of 15.4613 (Table 6), though the predicted R^2 (0.6893) was relatively lower, indicating slightly reduced external predictability. Among the terms evaluated, the volume of DMSO (B) had a significant influence on entrapment efficiency (F = 46.24, p = 0.0065), followed closely by the interaction term AB (F = 50.01, p = 0.0058), while the linear term A and quadratic terms A^2 and B^2 were not statistically significant ($p > 0.05$).

The regression equation obtained for entrapment efficiency was:

Entrapment Efficiency (R2) = 78.35 – 1.63A – 6.45B – 8.22AB + 2.02A^2 – 2.82B^2

The equation shows that DMSO volume and its interaction with Eudragit RL100 negatively influenced entrapment efficiency, suggesting a destabilizing effect at higher solvent volumes. The 2D contour plot and 3D response surface plot (Figures 5) illustrated a downward trend in entrapment efficiency with increasing DMSO, especially at higher polymer concentrations. The predicted vs. actual value closely followed the line of identity, supporting model accuracy. The perturbation plot indicated that DMSO volume was the dominant factor affecting drug entrapment, with sharper slope changes relative to Eudragit RL100 concentration.

Table 6: Fit summary of particle size and entrapment efficiency

Response	Source	Sequential p-value	Adjusted R^2	Predicted R^2	
Particle Size	Quadratic	0.0059	0.9257	0.6653	Suggested
Entrapment Efficiency	2FI	0.0022	0.8879	0.8067	Suggested

Table 7: ANOVA Summary for Quadratic Models of Particle Size (R1) and Entrapment Efficiency (R2) with Significance Levels of Formulation Variables

Source	Sum of Squares	df	Mean Square	F-value	p-value	
Particle Size						
Model	775.27	5	155.05	20.92	0.0154	significant
A-Eudragit RL100	0.5400	1	0.5400	0.0729	0.8047	Not significant
B-Volume of DMSO	48.17	1	48.17	6.50	0.0840	Not significant
AB	65.61	1	65.61	8.85	0.0588	Not significant
A^2	407.08	1	407.08	54.92	0.0051	significant
B^2	253.88	1	253.88	34.25	0.0099	significant
Residual	22.23	3	7.41			
Cor Total	797.50	8				
Entrapment Efficiency						
Model	559.86	5	111.97	20.73	0.0156	significant
A-Eudragit RL100	15.84	1	15.84	2.93	0.1853	Not significant
B-Volume of DMSO	249.74	1	249.74	46.24	0.0065	significant
AB	270.11	1	270.11	50.01	0.0058	significant
A^2	8.20	1	8.20	1.52	0.3056	Not significant
B^2	15.96	1	15.96	2.96	0.1841	Not significant
Residual	16.20	3	5.40			
Cor Total	576.06	8				

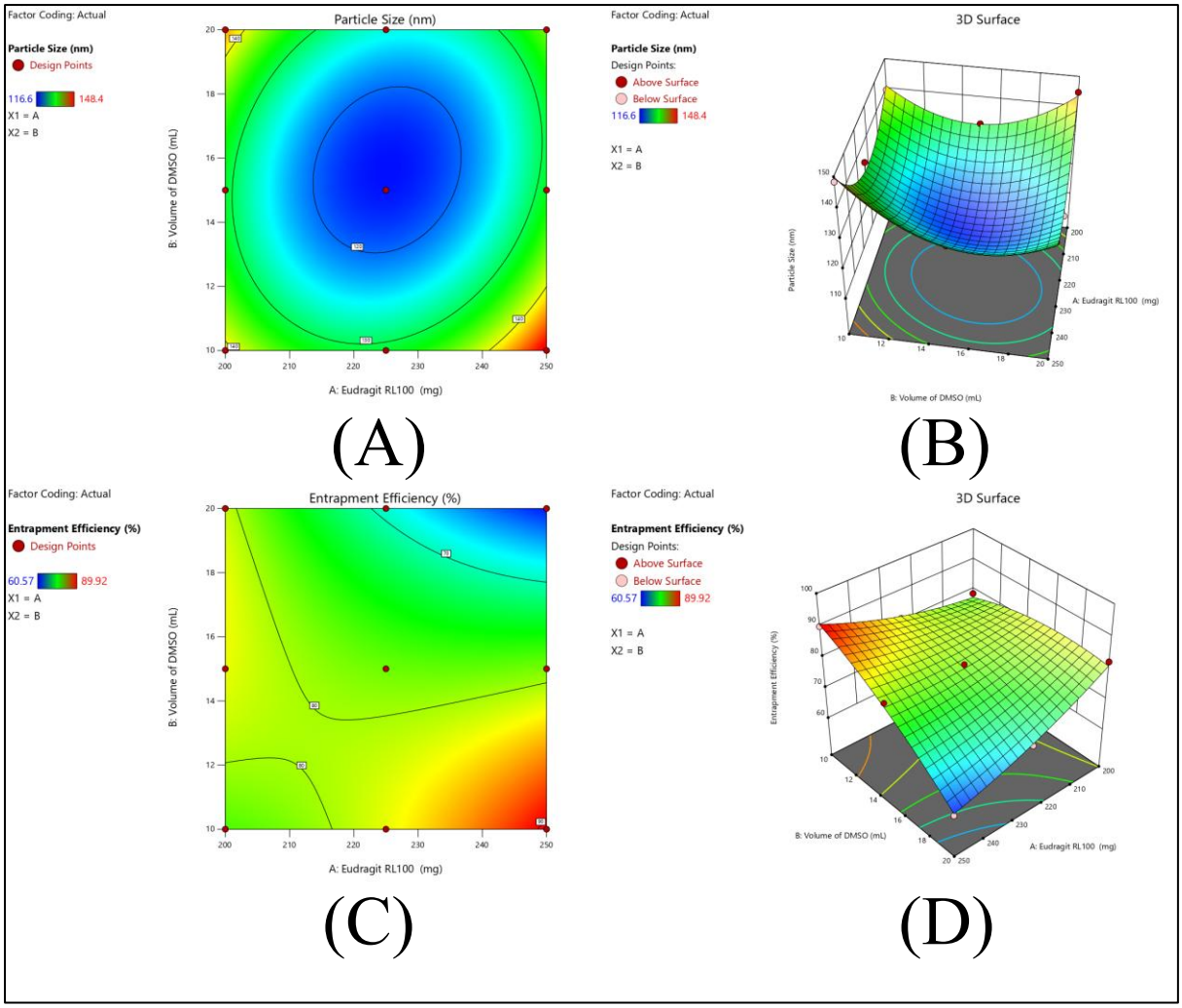

Figure 5: (A) Contour plot showing the effect of Eudragit RL100 concentration and DMSO volume on particle size of Baricitinib nanoparticles. The smallest particle size was observed at moderate levels of Eudragit RL100 and lower volumes of DMSO. (B): 3D surface plot representing the effect of Eudragit RL100 and DMSO volume on particle size. The plot shows a curved surface, indicating that both factors influence the particle size, with a clear minimum in the mid-range of the design space. (C): Contour plot showing how Eudragit RL100 and DMSO volume affect the entrapment efficiency of Baricitinib nanoparticles. Higher entrapment efficiency was observed at higher concentrations of Eudragit RL100 and lower volumes of DMSO. (D): 3D surface plot showing the response of entrapment efficiency to changes in Eudragit RL100 and DMSO volume. The surface shows a steep gradient, highlighting that entrapment efficiency decreases with increasing DMSO volume and is also affected by polymer concentration.

Validation of Statistical Model.

To validate the accuracy and predictive ability of the developed statistical model, an optimized formulation (NF5) was selected and experimentally evaluated. As shown in Table 8, the predicted particle size was 117.0 nm, while the experimental result was 116.6 nm, yielding a relative error of 0.4%. Similarly, the predicted entrapment efficiency was 77.46%, whereas the experimental value was 79.67%, with a relative error of -2.21%. These minor deviations confirm the robustness and reliability of the model for accurately predicting formulation outcomes.

Table 8: The predicted and experimental values of response variables and Observed error.

F. Code	Composition (%w/v)	Actual levels	Response	Predicted value	Experimental value	Relative Error
NF5	Eudragit RL100 (mg)	225	Particle Size (nm)	117.0	116.6	0.4
	Volume of DMSO (mL)	15				

NF5	Eudragit RL100	225	% Entrapment Efficiency	77.46	79.67	-2.21

Characterization of BCT-NPs loaded Transdermal patch

The physical evaluation of BCT-NPs loaded transdermal patches (Table 9) revealed that TNF4 exhibited the highest tensile strength (1.983 ± 0.13 kg/cm²) and folding endurance (221 ± 2.14), suggesting superior mechanical integrity and flexibility. The thickness ranged from 0.23 ± 0.02 mm to 0.29 ± 0.01 mm, with TNF4 being the thickest. Moisture absorption was highest in TNF4 (16.34 ± 0.73%) while TNF2 showed the lowest moisture content (3.7 ± 0.57%). These parameters confirm the successful fabrication and structural

Table 9: Evaluations of BCT-NPs loaded Transdermal patch

F. Code	Thickness (mm)	Tensile strength kg/cm²	Folding endurance	Moisture absorption/ uptake (%)	Moisture content (%)
TNF1	0.24±0.03	0.834±0.05	187±2.43	9.67±0.08	7.4±0.43
TNF2	0.23±0.02	1.432±0.07	193±1.21	14.43±0.87	3.7±0.57
TNF3	0.28±0.06	1.057±0.09	213±3.76	12.53±0.42	4.5±0.79
TNF4	0.29±0.01	1.983±0.13	221±2.14	16.34±0.73	8.2±0.89

Values are expressed in mean±SD, (n=3)

3.4.5. In Vitro Permeation Studies

The in vitro release profiles of BCT-NPs loaded transdermal patches demonstrated sustained drug release over 12 hours (Figure 6). Among all formulations, TNF3 exhibited the highest cumulative drug release (96.73%), followed by TNF4 (89.88%), TNF1 (89.23%), and TNF2 (83.29%) at 12 hours. Rapid initial release was observed in TNF4 and TNF2 within the first 6 hours, while TNF3 showed a more gradual and extended release. These findings indicate that TNF3 provided the most prolonged and consistent release profile, making it a suitable candidate for controlled transdermal drug delivery.

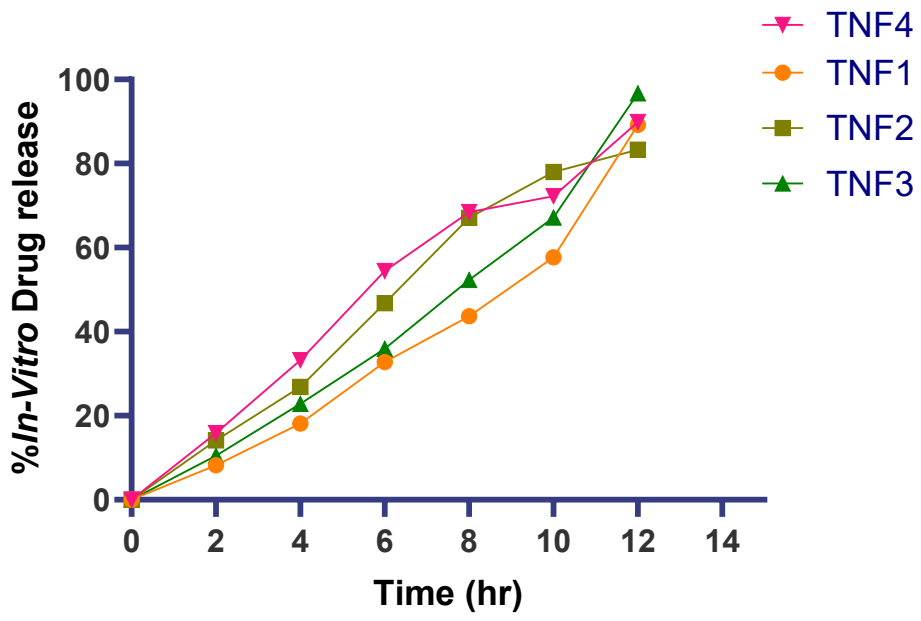

Figure 6: Graphical representation of the In Vitro Permeation Studies of BCT-NPs loaded Transdermal patch.

Release kinetics study

The in vitro drug release profile of the BCT-NPs loaded transdermal patch (TNF2) was evaluated using kinetic modeling (Figure 7). Among the models applied, the Zero-order model demonstrated the best fit with an R^2 value of 0.9816, indicating a concentration-independent, sustained drug release behavior. The Kors–Peppas model also exhibited a strong correlation (R^2 = 0.9419), suggesting anomalous diffusion as the probable release mechanism. Meanwhile, the Higuchi model (R^2 = 0.9100) supported a diffusion-controlled mechanism, and the First-order model showed a comparatively lower fit (R^2 = 0.9699). Overall, TNF2 followed a robust sustained release profile.

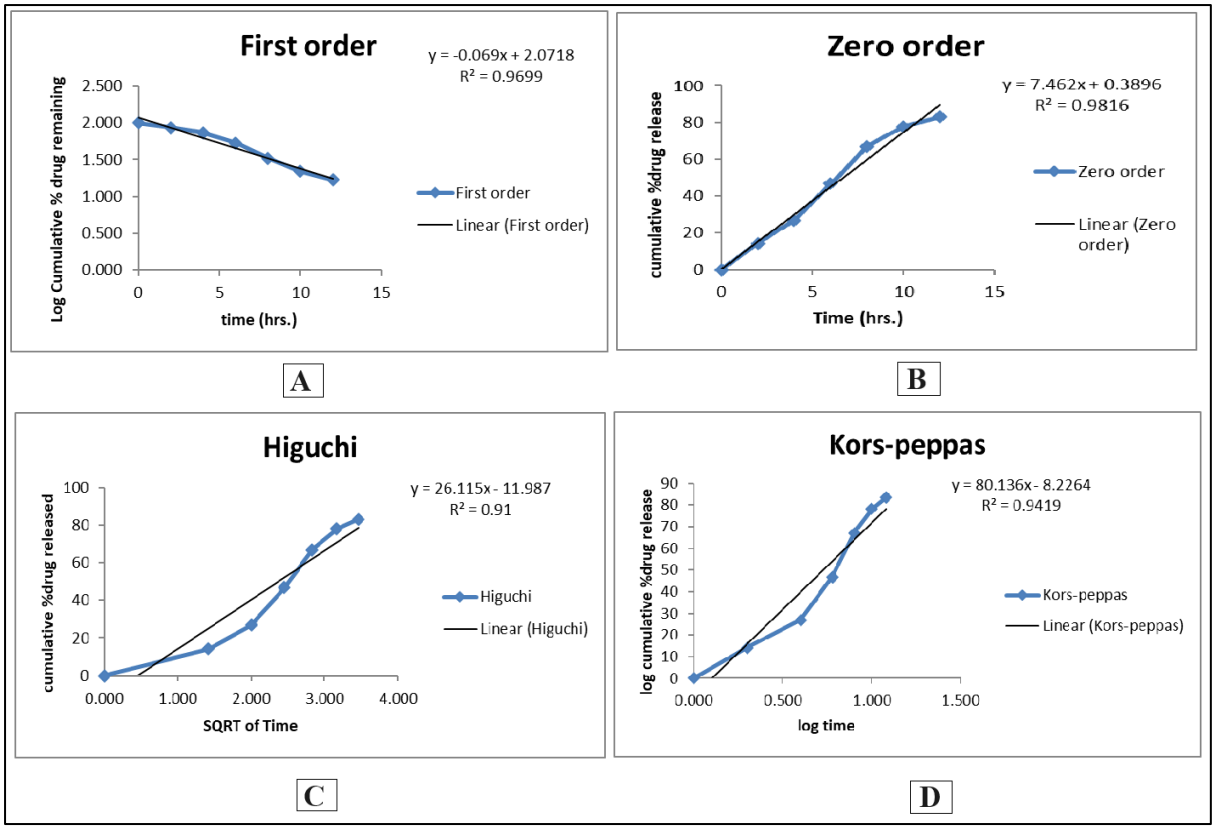

Figure 7: Release Kinetics of BCT-NPs loaded Transdermal patch TNF2 (A) First order, (B) Zero-order, (C) Higuchi model and (D) Kors- Peppas model.

Accelerated stability study

The accelerated stability study of the optimized BCT-NPs loaded transdermal patch (TNF2) showed no significant changes in physical appearance, confirming good structural integrity. Drug content slightly decreased from 98.32 ± 0.67% to 96.32 ± 0.85%, remaining within acceptable limits. Minor reductions were observed in patch thickness (0.23 ± 0.02 mm to 0.21 ± 0.01 mm), tensile strength, and folding endurance, while pH remained stable and skin-compatible (6.61 to 6.54). These findings indicate that the TNF2 patch maintained its mechanical properties, drug stability, and performance over 3 months under accelerated storage conditions.

Table 10: Accelerated Stability Study of BCT-NPs Loaded Transdermal Patch (TNF2)

Time (Months)	Physical Appearance	Thickness (mm)	Drug Content (%)	pH Value	Tensile Strength (kg/cm²)	Folding Endurance
0	Smooth, Transparent, Uniform	0.23 ± 0.02	98.32 ± 0.67	6.61 ± 0.03	1.432 ± 0.07	193 ± 1.21
1	No change	0.22 ± 0.01	97.68 ± 0.58	6.59 ± 0.04	1.415 ± 0.04	192 ± 1.46
2	No change	0.22 ± 0.02	96.89 ± 0.77	6.57 ± 0.06	1.402 ± 0.05	190 ± 2.02
3	No change	0.21 ± 0.01	96.32 ± 0.85	6.54 ± 0.05	1.395 ± 0.03	189 ± 1.37

All values are expressed as mean ± SD, n = 3.

DISCUSSION

The present investigation was aimed at developing a stable, efficient, and patient-compliant transdermal drug delivery system of Baricitinib through nanoparticle-based incorporation in polymeric patches [40]. The strategy focused on enhancing the solubility and sustained delivery of Baricitinib, a poorly water-soluble drug, by designing nanoparticles (BCT-NPs) using Eudragit RL100 via a nanoprecipitation technique [41]. The solubility study (Table 4) revealed that Baricitinib demonstrated highest solubility in DMSO (74.0 ± 1.0 mg/mL), followed by methanol (21.4 ± 0.6 mg/mL), whereas negligible solubility

was observed in aqueous media, such as distilled water and phosphate buffer (≤0.46 mg/mL) [42]. These results justified the use of DMSO as an organic solvent during nanoparticle fabrication to maximize drug loading. The prepared BCT-NPs (NF1–NF9) were subjected to thorough characterization [43]. Among the formulations, NF5 emerged as the optimized batch based on its desirable particle size (116.6 ± 10.3 nm), high entrapment efficiency (79.67 ± 2.45%), and favorable zeta potential (−39.32 mV) (Table 5) [44]. Statistical analysis using a quadratic model showed excellent model fitting for both response variables, with high R^2 values of 0.9925 for particle size and 0.9719 for entrapment efficiency (Tables 6 and 8). ANOVA further revealed that quadratic terms (A^2 and B^2) significantly influenced particle size ($p < 0.01$), whereas interaction term AB and solvent volume (B) significantly affected drug entrapment ($p < 0.01$), as per Table 7. The low prediction error in NF5's particle size (0.4%) and entrapment efficiency (−2.21%) confirmed the validity of the model predictions [45].

Compatibility assessments by FTIR and DSC confirmed the absence of major physicochemical interactions between Baricitinib and excipients. The characteristic peaks of Baricitinib remained unchanged in the physical mixture spectra, supporting excipient compatibility (Figure 4). Similarly, thermal analysis revealed two distinct peaks in the physical mixture one near the melting point of Baricitinib and another corresponding to polymer transitions indicating no significant interaction (Figure 3) [46].

The optimized BCT-NPs were incorporated into polymeric transdermal patches using HPMC K15M and PVP as matrix-forming agents [47]. Among four patch formulations (TNF1–TNF4), TNF2 exhibited superior mechanical and physicochemical characteristics: high tensile strength (1.432 ± 0.07 kg/cm²), moderate folding endurance (193 ± 1.21), and acceptable moisture uptake and content (Table 9). These attributes suggest that TNF2 provides suitable mechanical integrity and flexibility for skin application, while preventing excessive hydration or brittleness. The in vitro release studies over 12 hours demonstrated controlled and sustained drug release from all formulations [48,49]. TNF2 achieved 83.29% cumulative release and best fit the zero-order kinetic model ($R^2 = 0.9816$), suggesting a consistent release rate over time (Table 11). The Kors–Peppas model ($R^2 = 0.9419$) also showed a good fit, indicating that drug release may be governed by a combination of diffusion and erosion mechanisms (Figure 7) [50]. The performance of TNF2 makes it the most promising candidate for transdermal Baricitinib delivery. Furthermore, accelerated stability studies of TNF2 confirmed its robustness over a 3-month period. No significant changes were observed in drug content, pH, thickness, tensile strength, or moisture content, affirming the physical and chemical stability of the formulation under stress conditions (Table 12) [51].

CONCLUSION

The present study successfully developed and optimized Baricitinib-loaded nanoparticles (BCT-NPs) using Eudragit RL100 via a nanoprecipitation method and incorporated them into transdermal patches using a solvent casting technique. Among the prepared batches, TNF2 exhibited superior mechanical strength, folding endurance, and sustained drug release up to 12 hours, best fitting the zero-order kinetic model. The optimized formulation remained stable under accelerated conditions, indicating good shelf life and formulation robustness. These findings suggest that the BCT-NPs loaded transdermal patch offers a promising platform for sustained delivery of Baricitinib, potentially enhancing patient compliance and therapeutic efficacy in chronic inflammatory conditions like rheumatoid arthritis. Future studies should focus on in vivo pharmacokinetic and pharmacodynamic evaluations to validate the clinical translation and therapeutic advantage of the optimized transdermal formulation.

Abbreviations

ANOVA: Analysis of Variance; FTIR: Fourier-transform Infrared Spectroscopy; UV: Ultraviolet Spectroscopy; DLS: Dynamic Light Scattering; DSC: Differential Scanning Calorimetry; EE: Entrapment Efficiency; ZP: Zeta Potential; PVA: Polyvinyl Alcohol; DMSO: Dimethyl Sulfoxide; PBS: Phosphate Buffer Saline; SD: Standard Deviation; rpm: Revolutions Per Minute; HPMC: Hydroxypropyl Methylcellulose; PVP: Polyvinylpyrrolidone; PEG: Polyethylene Glycol; RT: Room Temperature; BCT-NPs: Baricitinib-loaded Nanoparticles; TNF: Transdermal Nanoparticle Film; R^2: Coefficient of Determination; Fig.: Figure; RH: Relative Humidity; nm: Nanometer; mg/mL: Milligrams per Milliliter; min: Minutes; °C: Degree Celsius; Df: Degree of Freedom.

REFERENCES

1. Safiri S, Kolahi AA, Hoy D, Smith E, Bettampadi D, Mansournia MA, et al. Global, regional and national burden of rheumatoid arthritis 1990-2020: a systematic analysis of the Global Burden of Disease study 2021. Ann Rheum Dis. 2023;82(1):108-120. doi: 10.1136/ard-2022-223522
2. World Health Organization. Rheumatoid arthritis: Key facts [Internet]. Geneva: World Health Organization; 2023 [cited 2024 Jan 15]. Available from: https://www.who.int/news-room/fact-sheets/detail/rheumatoid-arthritis
3. Singh JA, Saag KG, Bridges SL Jr, Akl EA, Bannuru RR, Sullivan MC, et al. 2015 American College of Rheumatology guideline for the treatment of rheumatoid arthritis. Arthritis Rheumatol. 2016;68(1):1-26. doi: 10.1002/art.39480
4. Smolen JS, Landewé RBM, Bijlsma JWJ, Burmester GR, Dougados M, Kerschbaumer A, et al. EULAR recommendations for the management of rheumatoid arthritis with synthetic and biological disease-modifying antirheumatic drugs: 2019 update. Ann Rheum Dis. 2020;79(6):685-699. doi: 10.1136/annrheumdis-2019-216655
5. Gibofsky A. Overview of epidemiology, pathophysiology, and diagnosis of rheumatoid arthritis. Am J Manag Care. 2012;18(13 Suppl):S295-302. PMID: 23327517
6. Taylor PC, Weinblatt ME, Burmester GR, Rooney TP, Witt S, Walls CD, et al. Cardiovascular safety during treatment with baricitinib in rheumatoid arthritis. Arthritis Rheumatol. 2019;71(7):1042-1055. doi: 10.1002/art.40841
7. Fridman JS, Scherle PA, Collins R, Burn TC, Li Y, Li J, et al. Selective inhibition of JAK1 and JAK2 is efficacious in rodent models of arthritis: preclinical characterization of INCB028050. J Immunol. 2010;184(9):5298-5307. doi: 10.4049/jimmunol.0902819
8. Genovese MC, Kremer J, Zamani O, Ludivico C, Krogulec M, Xie L, et al. Baricitinib in patients with refractory rheumatoid arthritis. N Engl J Med. 2016;374(13):1243-1252. doi: 10.1056/NEJMoa1507247
9. Fleischmann R, Schiff M, van der Heijde D, Ramos-Remus C, Spindler A, Stanislav M, et al. Baricitinib, methotrexate, or combination in patients with rheumatoid arthritis and no or limited prior disease-modifying antirheumatic drug treatment. Arthritis Rheumatol. 2017;69(3):506-517. doi: 10.1002/art.39953
10. Dougados M, van der Heijde D, Chen YC, Greenwald M, Drescher E, Liu J, et al. Baricitinib in patients with inadequate response or intolerance to conventional synthetic DMARDs: results from the RA-BUILD study. Ann Rheum Dis. 2017;76(1):88-95. doi: 10.1136/annrheumdis-2016-210094
11. Prausnitz MR, Langer R. Transdermal drug delivery. Nat Biotechnol. 2008;26(11):1261-1268. doi: 10.1038/nbt.1504
12. Silva AC, Kumar A, Wild W, Ferreira D, Santos D, Forbes B. Long-term stability, biocompatibility and oral toxicity of resveratrol-loaded solid lipid nanoparticles. Int J Pharm. 2012;436(1-2):703-712. doi: 10.1016/j.ijpharm.2012.07.027
13. Brown MB, Martin GP, Jones SA, Akomeah FK. Dermal and transdermal drug delivery systems: current and future prospects. Drug Deliv. 2006;13(3):175-187. doi: 10.1080/10717540500455975
14. Patel MR, Patel RB, Parikh JR, Solanki AB, Patel BG. Effect of formulation components on the in vitro permeation of microemulsion drug delivery system of fluconazole. AAPS PharmSciTech. 2009;10(3):917-923. doi: 10.1208/s12249-009-9280-4
15. Kim YC, Park JH, Prausnitz MR. Microneedles for drug and vaccine delivery. Adv Drug Deliv Rev. 2012;64(14):1547-1568. doi: 10.1016/j.addr.2012.04.005
16. ICH Expert Working Group. ICH Q2(R1) Validation of analytical procedures: text and methodology. ICH Harmonised Tripartite Guideline. Geneva: International Conference on Harmonisation of Technical Requirements for Registration of Pharmaceuticals for Human Use; 2005.
17. Yalkowsky SH, He Y, Jain P. Handbook of aqueous solubility data. 2nd ed. Boca Raton: CRC Press; 2010.
18. Jouyban A. Handbook of solubility data for pharmaceuticals. Boca Raton: CRC Press; 2010.
19. Ford JL, Timmins P. Pharmaceutical thermal analysis: techniques and applications. New York: Ellis Horwood; 1989.
20. Brittain HG. Polymorphism in pharmaceutical solids. 2nd ed. New York: Informa Healthcare; 2009.
21. Silverstein RM, Webster FX, Kiemle DJ, Bryce DL. Spectrometric identification of organic compounds. 8th ed. New York: John Wiley & Sons; 2014.
22. Stuart BH. Infrared spectroscopy: fundamentals and applications. New York: John Wiley & Sons; 2004.
23. Montgomery DC. Design and analysis of experiments. 8th ed. New York: John Wiley & Sons; 2012.
24. Box GEP, Hunter JS, Hunter WG. Statistics for experimenters: design, innovation, and discovery. 2nd ed. New York: John Wiley & Sons; 2005.
25. Myers RH, Montgomery DC, Anderson-Cook CM. Response surface methodology: process and product optimization using designed experiments. 4th ed. New York: John Wiley & Sons; 2016.
26. Fessi H, Puisieux F, Devissaguet JP, Ammoury N, Benita S. Nanocapsule formation by interfacial polymer deposition following solvent displacement. Int J Pharm. 1989;55(1):R1-R4. doi: 10.1016/0378-5173(89)90281-0
27. Vauthier C, Bouchemal K. Methods for the preparation and manufacture of polymeric nanoparticles. Pharm Res. 2009;26(5):1025-1058. doi: 10.1007/s11095-008-9800-3
28. Almeida AJ, Souto E. Solid lipid nanoparticles as a drug delivery system for peptides and proteins. Adv Drug Deliv Rev. 2007;59(6):478-490. doi: 10.1016/j.addr.2007.04.007
29. Malvern Instruments Ltd. Zetasizer Nano series user manual. Malvern: Malvern Instruments Ltd; 2013.
30. Costa P, Sousa Lobo JM. Modeling and comparison of dissolution profiles. Eur J Pharm Sci. 2001;13(2):123-133. doi: 10.1016/s0928-0987(01)00095-1
31. Mukherjee B, Mahapatra S, Gupta R, Patra B, Tiwari A, Arora P. A comparison between povidone-ethylcellulose and povidone-eudragit transdermal dexamethasone matrix patches based on in vitro skin permeation. Eur J Pharm Biopharm. 2005;59(3):475-483. doi: 10.1016/j.ejpb.2004.09.009
32. Indian Pharmacopoeia Commission. Indian Pharmacopoeia 2018. Vol 1. Ghaziabad: Indian Pharmacopoeia Commission; 2018.
33. United States Pharmacopeial Convention. United States Pharmacopeia and National Formulary (USP 43-NF 38). Rockville: United States Pharmacopeial Convention; 2020.
34. British Pharmacopoeia Commission. British Pharmacopoeia 2020. London: The Stationery Office; 2020.

35. American Society for Testing and Materials. ASTM D882-18 Standard test method for tensile properties of thin plastic sheeting. West Conshohocken: ASTM International; 2018.
36. Rowe RC, Sheskey PJ, Quinn ME, editors. Handbook of pharmaceutical excipients. 6th ed. London: Pharmaceutical Press; 2009.
37. International Conference on Harmonisation of Technical Requirements for Registration of Pharmaceuticals for Human Use. ICH Q1A(R2) Stability testing of new drug substances and products. Geneva: ICH; 2003.
38. Franz TJ. Percutaneous absorption: on the relevance of in vitro data. J Invest Dermatol. 1975;64(3):190-195. doi: 10.1111/1523-1747.ep12533356
39. Higuchi T. Mechanism of sustained-action medication. Theoretical analysis of rate of release of solid drugs dispersed in solid matrices. J Pharm Sci. 1963;52(12):1145-1149. doi: 10.1002/jps.2600521210
40. Gao Y, Li LB, Zhai G. Preparation and characterization of Pluronic/TPGS mixed micelles for solubilization of camptothecin. Colloids Surf B Biointerfaces. 2008;64(2):312-318. doi: 10.1016/j.colsurfb.2008.02.007
41. Mora-Huertas CE, Fessi H, Elaissari A. Polymer-based nanocapsules for drug delivery. Int J Pharm. 2010;385(1-2):113-142. doi: 10.1016/j.ijpharm.2009.10.018
42. Aulton ME, Taylor KMG, editors. Aulton's pharmaceutics: the design and manufacture of medicines. 5th ed. Edinburgh: Churchill Livingstone; 2018.
43. Letchford K, Burt H. A review of the formation and classification of amphiphilic block copolymer nanoparticulate structures: micelles, nanospheres, nanocapsules and polymersomes. Eur J Pharm Biopharm. 2007;65(3):259-269. doi: 10.1016/j.ejpb.2006.11.009
44. Panyam J, Labhasetwar V. Biodegradable nanoparticles for drug and gene delivery to cells and tissue. Adv Drug Deliv Rev. 2003;55(3):329-347. doi: 10.1016/s0169-409x(02)00228-4
45. Soppimath KS, Aminabhavi TM, Kulkarni AR, Rudzinski WE. Biodegradable polymeric nanoparticles as drug delivery devices. J Control Release. 2001;70(1-2):1-20. doi: 10.1016/s0168-3659(00)00339-4
46. Craig DQM. The mechanisms of drug release from solid dispersions in water-soluble polymers. Int J Pharm. 2002;231(2):131-144. doi: 10.1016/s0378-5173(01)00891-2
47. Raghavan SL, Trividic A, Davis AF, Hadgraft J. Crystallization of hydrocortisone acetate: influence of polymers. Int J Pharm. 2001;212(2):213-221. doi: 10.1016/s0378-5173(00)00610-0
48. Siepmann J, Peppas NA. Modeling of drug release from delivery systems based on hydroxypropyl methylcellulose (HPMC). Adv Drug Deliv Rev. 2001;48(2-3):139-157. doi: 10.1016/s0169-409x(01)00112-0
49. Ritger PL, Peppas NA. A simple equation for description of solute release II. Fickian and anomalous release from swellable devices. J Control Release. 1987;5(1):37-42. doi: 10.1016/0168-3659(87)90035-6
50. Dash S, Murthy PN, Nath L, Chowdhury P. Kinetic modeling on drug release from controlled drug delivery systems. Acta Pol Pharm. 2010;67(3):217-223. PMID: 20524422
51.ICH Expert Working Group. ICH Q1A(R2) Stability testing of new drug substances and products. ICH Harmonised Tripartite Guideline. Geneva: International Conference on Harmonisation of Technical Requirements for Registration of Pharmaceuticals for Human Use; 2003.